Magnetic Resonance Imaging and Mathematical Modeling of Progressive Formalin Fixation of the Human Brain

Charlotte J. Yong-Hing,[1] Andre Obenaus,[2] Rodrick Stryker,[3] Karen Tong,[4] and Gordon E. Sarty,[5]*

The temporal magnetic resonance (MR) appearance of human brain tissue during formalin fixation was measured and modeled using a diffusion mathematical model of formalin fixation. Coronal MR images of three human brains before formalin fixation and at multiple time points thereafter were acquired. T_1 relaxation, T_2 relaxation, water apparent diffusion coefficient (ADC), and proton density (PD) maps were calculated. The size of a light "formalin band" region, visible in T_1 weighted images, was compared to a mathematical model of diffusive mass transfer of formalin into the brain. T_1 relaxation, T_2 relaxation, and PD all decreased, in both gray and white matter, as formalin fixation progressed. The ADC remained more or less constant. The location of the inner boundary of the formalin band followed a time course consistent with the steepest formalin concentration gradient in the mathematical model. Based on the diffusion model, the brain is not completely saturated in formalin until after 14.8 weeks of formalin immersion and, based on the observed changes in T_1, T_2, and PD, fixation is not complete until after 5.4 weeks. During fixation, the ongoing attenuation of T_1 relaxation, T_2 relaxation, and PD must be taken into consideration when performing postmortem MRI studies. Magn Reson Med 54:324–332, 2005. © 2005 Wiley-Liss, Inc.

Key words: MRI; forensic pathology; brain; diffusion; postmortem

Postmortem magnetic resonance (MR) imaging is widely used to make pathologic diagnoses and also for a wide range of research. However, the tissue changes induced by fixation methods may influence the findings. To date only a handful of human and animal studies have described MR signal changes in fixed tissue and none of these changes have been quantified with physically based mathematical models. An MR spectroscopy study of rat muscle, intestine, fatty tissue, cerebral cortex, and white matter showed that relaxation parameters change considerably after fixation of the tissues (1). Another study found that T_1 and T_2 relaxation times of rat liver and spleen were reduced after formalin fixation (2). Two studies have investigated MR signal change in spinal cord tissue with fixation: diffusion anisotropy is maintained in white matter tracts of cat spinal cords as a function of fixation (3), T_1 relaxation, T_2 relaxation, and spin-density values for rat and human cervical spinal cords decrease considerably after formalin fixation (4). A reduction in T_2 relaxation values and an increase in spin-density values with formalin fixation have been demonstrated in human brain tissue (5). The changes in T_1 relaxation, apparent diffusion coefficient (ADC), and proton density (PD) values of human brain tissue after formalin fixation have never been formally reported. In addition, a lighter band of tissue, apparently related to the diffusion of formalin into the brain, has been observed by several investigators but has not been mathematically modeled to the best of our knowledge (5). If not taken into consideration, such changes may lead to artificial results and misdiagnosis. The present study was designed to further investigate how MR appearance and parameters of brain tissue change over time as formalin fixation proceeds and to find a plausible physical explanation of the lighter "formalin band " seen in T_1 weighted images by fitting the data to a mathematical model of formalin diffusion.

METHODS

Subjects

Three human brains were obtained from the Pathology Department at the Royal University Hospital in Saskatoon within 2 h of death. The brains, without dura matter, were removed from the skulls prior to imaging. The subjects were adults who had no overt brain pathology or trauma. Average age at death was 61 years. Written consent was obtained from the families of the deceased for autopsy and for the use of the brains for this study.

Image Acquisition

The brains were placed with the frontal lobes facing into the bore of the MR imager (Siemens SP, Erlangen, Germany) on moistened saline towels, at room temperature (20°C), to raise them into the center of the field of view. A cardboard "frame" with a cutout for the brain was placed in the coronal plane at the level of the motor cortex for guiding the placement of vitamin E pills as fiducial markers, which remained in place for the duration of the study. Three markers were placed in the motor cortex of each brain in the coronal plane along the cardboard frame at right, left, and midline locations. An axial scout image was acquired to identify the markers and then coronal images were lined up to the plane of the markers to ensure consistent slice positions at all time points. Coronal MR im-

[1]Radiology and Diagnostic Imaging, University of Alberta Hospital, Edmonton, Alberta, Canada.

[2]Department of Radiation Medicine, Loma Linda University, Loma Linda, California, USA.

[3]Internal Medicine, University of Saskatchewan, Saskatoon, Saskatchewan, Canada.

[4]Department of Radiology, Loma Linda University, Loma Linda, California, U.S.A.

[5]Psychology, University of Saskatchewan, Saskatoon, Saskatchewan, Canada.

Grant sponsor: Saskatchewan Health Services and Utilization Research Council; Grant sponsor: Canadian Institutes for Health Research.

*Correspondence to: G. E. Sarty, Department of Psychology, University of Saskatchewan, 9 Campus Drive, Saskatoon, Saskatchewan S7N 5A5, Canada., E-mail: gordon.sarty@usask.ca

Received 19 March 2004; revised 15 March 2005; accepted 15 March 2005.

DOI 10.1002/mrm.20578

Published online in Wiley InterScience (www.interscience.wiley.com).

ages were taken before fixation (0 h) and then the brains were fixed in formalin solution (immersion, 20% phosphate buffered formalin) and images were taken at 4, 10, 18, 34, 42, 58, 66, 84, 90, 108, 114, 130, 140, 165, 187, 210, 234, 258, 282, 308, and 514 h for brain 1; 19, 34, 42, 66, 90, 114, 138, 186, 254, 302, 350, and 518 h for brain 2; and 18, 42, 66, 90, 114, 165, 234, 350, and 514 h for brain 3. Images were acquired with a Siemens SP 1.5-T imager using T_1-weighted, multiple echo T_2-weighted, and water diffusion weighted sequences. T_1 relaxation maps, PD maps, T_2 relaxation maps, and ADC maps were calculated. The T_1-weighted images with T_R = 600, 700, 800, and 1500 ms and T_E = 15 ms were used for the calculation of the T_1 and PD maps. These choices for T_R began with the recommended value of 600 ms for miscellaneous brain imaging in a clinical setting (6) but it is recognized that the closely spaced T_R values were not optimal given the final T_1 values computed; however, the T_R choices lead to images having similar automatically set receiver gains. 16 echo T_2-weighted images with T_E = 20, 40, 55, 70, 85, 100, 115, 130, 145, 160, 175, 190, 205, 220, 235, and 250 ms and T_R = 2200 ms were used for the calculation of the T_2 maps. Given the T_1 values subsequently found in this study, a longer T_R for the multiple echo T_2 data would provide a higher signal-to-noise ratio in any subsequent work. A pair of water diffusion weighted and unweighted images with T_E = 81 ms and T_R = 2200 ms were also acquired. The water ADC maps were computed from two sequences with diffusion gradients, in the axial *z*-direction, giving *b* values of 0 and 177.76 s/mm^2, where $b = \gamma^2\delta^2(\Delta - \delta/3)G^2$, γ = gyromagnetic ratio of the proton, δ = the temporal length of individual diffusion gradient applications, Δ = temporal spacing between the initiation of each diffusion gradient pulse, and G = the strength of the gradient pulse. For this work δ = 30 ms, Δ = 37.5 ms, and G = 10 mT/m were used. The resulting relatively low *b* value was therefore due to the limited maximum gradient of 10 mT/m available on the imager. The image slice containing the fiducial markers (and the motor cortex) was chosen for MR signal change analysis. This slice was chosen for analysis based on visualization of and differentiation between white and gray matter.

The T_1 and PD maps were computed by minimizing the sum of square differences between the data values and the following pixel-wise signal model, evaluated at the acquired T_R values

$$S(T_R) = \rho(1 - \exp(-T_R/T_1)), \quad [1]$$

where $S(T_R)$ is the image gray scale pixel value for the T_1-weighted image acquired with repeat time T_R and ρ is the PD in arbitrary units. The T_2 maps were computed by minimizing the sum of square differences between the data values and the following pixel-wise signal model, evaluated at the acquired T_E values

$$S(T_E) = \rho\ \mathrm{xp}(-T_E/T_2), \quad [2]$$

where $S(T_E)$ is the image gray scale pixel value for the T_2-weighted image acquired with echo time T_E and ρ (not used) is proportional to proton density and T_1 recovery due to the relatively short T_R used. The ADC maps, D_a, were computed as

$$D_a = -\frac{1}{b}\ln\left(\frac{W}{U}\right), \quad [3]$$

where W is the diffusion weighted image and U is the unweighted image. Stock imaging sequences were used to collect all images and these sequences automatically set the receiver gain. Therefore three methods were used to compute the PD/T_1 and ADC maps: (1) using unmodified data in Eqs. [1]. and [3], (2) scaling the image values by the ratio of receiver gains recorded in the image headers, and (3) scaling the image values by the ratios of noise amplitudes measured from the background of the images. The recorded gains were found to be all very similar and no significant differences were found in map values between the maps computed with the three different scaling corrections. Therefore, the random bias in the map values from the unknown receiver gains was of the same order of magnitude, or smaller, than the noise in the data. The results reported are based on the maps computed from unscaled data so it is possible that a small random bias exists in the absolute values of the T_1 and ADC values computed. All maps were computed using locally written software (in C). Least squares were computed using bisection. For each pixel curve fit used to produce the maps of Eqs. [1] and [2], a χ^2 value could be computed as

$$\chi^2 = \sum_i \frac{(O_i - E_i)^2}{E_i}, \quad [4]$$

where O_i is the observed image *i* gray scale value and E_i is the expected value as given by Eq. [1] or [2]. Typical values for the PD/T_1 maps were $\chi^2 = 1$ ($P = 0.8$) with a maximum of approximately $\chi^2 = 4$ ($P = 0.3$). The fits for the T_2 data were not explicitly computed, because the values of ρ from Eq. [2] were not recorded, but, since the T_1-weighted and T_2-weighted images had similar signal-to-noise ratios, the T_2 fits would be expected to be better than the T_1 fits as a result of using more data points per fit (less effect of outliers). Therefore, our suboptimal choices of T_E values for the T_1 data and T_R values for the T_2 data did not lead to T_1 and T_2 estimates with low signal-to-noise ratios.

Signal Change Analysis

Multiple regional analyses of pixel intensity of gray and white matter and their change over time were performed on the coronal maps using the Cheshire (Parexel International Corp.) image analysis program. At selected locations in gray and white matter regions, four regions of interest (ROIs) were plotted on the PD images or T_2 maps. Figure 1a shows how the ROIs were placed in a straight line from the surface of the brain inward at approximately 2, 6, 10 and 14 mm from the surface of the cortex. The ROIs were propagated to the remaining two maps and to a T_1-weighted image (T_R = 600) to verify anatomic placement. The most superficial ROIs were placed 1 to 2 pixels from the external surface of the brain, and the deepest ROIs were placed 30 pixels from the external surface of brain.

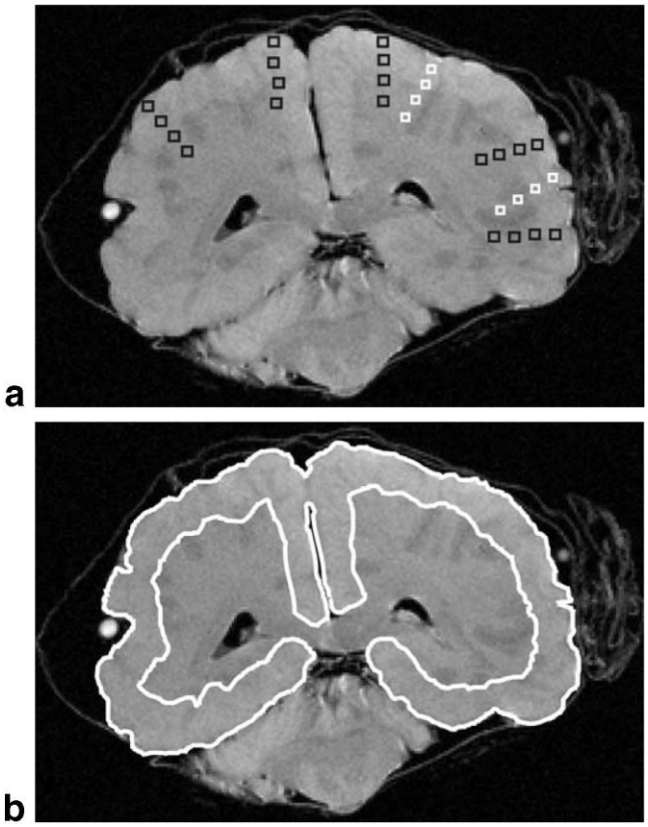

FIG. 1. T_1-weighted image of brain 3 at 66 h showing analysis ROIs. (**a**) Sets of four ROIs were traced in both white and gray matter, black ROIs for gray matter and white ROIs for white matter. The ROIs were propagated between the T_1-weighted images and the four parameter maps for the quantification of T_1, T_2, PD, and ADC. (**b**) The band of formalin-fixed tissue appears lighter than the surrounding tissue and is outlined in white. The outlined region was used to compute the area of the lighter tissue. The entire cerebral cortex, not including the ventricles, was similarly outlined for area ratio computation.

The map values within the ROIs were calculated and recorded. The mean map value of the corresponding ROIs, across all three brains, at each depth was calculated for both gray and white matter. This resulted in average map values for ROI 1, 2, 3, and 4 at approximately 2, 6, 10, and 14 mm depth, respectively, for T_1 relaxation, T_2 relaxation, PD, and ADC for both gray and white matter. For each of the 32 resulting time series, an exponential curve of the form

$$y = a_1(1 - \exp(-a_2\, t)) + a_3 \qquad [5]$$

was fit using the method of least squares regression, where y is the map value at time point t. The curve of Eq. [5] is the simplest one that tends to an asymptote; the curve begins at a_3 and exponentially changes to an asymptote of a_1+a_3. The parameter $1/a_2$ is the time constant of the change; the change is 99% complete after $5/a_2$.

Formalin Band/Whole Brain Ratio Tracing and Calculations

Coronal T_1-weighted images (T_R = 600) were used to visualize the progressive fixation of the brain. The slices chosen for the area measurements were the slices in which the fiducial markers were visible. When the vitamin E markers were visible in more than one slice, measurements were taken from all images that contained the marker and averaged. When the markers were not visible on any of the images, the image used was the one that corresponded most anatomically with the slices chosen for the previous and subsequent time points. On T_1-weighted images, the area apparently fixed by formalin, the formalin band, appeared lighter than adjacent tissue. The brain areas were outlined semi-automatically using Cheshire; maximum and minimum threshold values were determined and then used to automatically outline the entire brain. The outlines were adjusted to exclude the cerebellum and pons. Figure 1b shows how the area of the formalin band was finally outlined.

The areas of brain hemispheres and of the lighter formalin band were calculated and the values were transferred to a spreadsheet for analysis. The formalin band area was divided by the total hemisphere area to obtain an area ratio for each time point. When two images were used for measurements at a single time point, the formalin areas were summed and divided by summed hemisphere areas to obtain a single ratio. The ratios of the areas of the formalin band to the rest of the brain were plotted over time to quantify the formalin band progression. The area ratios, m, were converted to normalized radius values, r, using

$$r = \sqrt{1 - m}. \qquad [6]$$

The normalized radius represents the radius of the formalin band as a fraction of the radius from the center of the brain to the cortex surface. Equation [6] normalizes, or registers, the brain onto a unit sphere as may be seen from the following argument. Let A_o represent the area of the whole brain in the image and let $A_o - A_i$ represent the area of the formalin band. Pick R_o and R_i such that $A_o = \pi\, R_o{}^2$ and $A_i = \pi\, R_i{}^2$ (the radii of circles with equivalent areas). Then

$$m = \frac{\pi R_o{}^2 - \pi R_i{}^2}{\pi R_o{}^2} = \frac{R_o{}^2 - R_i{}^2}{R_o{}^2} \qquad [7]$$

so that

$$1 - m = \frac{R_i{}^2}{R_o{}^2}. \qquad [8]$$

So r of Eq. [6] represents the ratio of inner radius to outer radius of the formalin band represented as a band on a circular cross-section of a spherical brain.

Diffusion Math Model

Approximating the brain as a solid sphere, we may use Fick's law of diffusion to model diffusion of formalin into the brain. Fick's first law of diffusion (7) states that the rate of mass transfer per unit area, **J**, is proportional to the gradient of the concentration c,

$$\mathbf{J} = -D\nabla c, \qquad [9]$$

where the constant of proportionality, D, is the diffusion coefficient. Expressing **J** in Eq. [9] in terms of concentration leads to Fick's second law, the parabolic differential equation

$$\frac{\partial c}{\partial t} = D\left[\frac{\partial^2 c}{\partial x^2} + \frac{\partial^2 c}{\partial y^2} + \frac{\partial^2 c}{\partial z^2}\right], \quad [10]$$

written here in Cartesian coordinates (x,y,z). Assuming spherical symmetry and changing to polar spherical coordinates (r,θ,ϕ), Eq. [10] becomes

$$\frac{1}{D}\frac{\partial c}{\partial t} = \frac{\partial^2 c}{\partial r^2} + \frac{2}{r}\frac{\partial c}{\partial r}, \quad [11]$$

where, for our spherical brain model, c represents the formalin concentration, r the radius, t the time, and D the diffusion coefficient. With an initial concentration of c_1 outside the brain and 0 inside the brain, Eq. [11] may be solved by standard separation of variable techniques, where the solution is expressed as a Fourier series and a solution for the series coefficients computed (8), to yield

$$c(r,t) = c_1 + \frac{2Rc_1}{\pi}\sum_{n=1}^{\infty}\frac{(-1)^n}{nr}\sin\left[\frac{n\pi r}{R}\right]\exp\left[\frac{-n^2\pi^2 D}{R^2}t\right], \quad [12]$$

where R is the radius of the ideal spherical brain. By assuming that $R = 1$, which we may compare to the measured normalized formalin band radius, setting $c_1 = 1$ (so that the formalin concentration is in normalized units) and setting $t_1 = t/D$ and dropping the subscript on the new scaled t, Eq. [12] simplifies to

$$c(r,t) = 1 + \frac{2}{\pi}\sum_{n=1}^{\infty}\frac{(-1)^n}{nr}\sin[n\pi r]\exp[-n^2\pi^2 t]. \quad [13]$$

In this model, the concentration c is essentially 1 at $t = 1$ based on numerical evaluation of Eq. [13]. That is, the brain may be regarded as maximally saturated at $t = 1$. Computer animations of the solution of Eq. [13] and its spatial derivatives reveal that the temporal behavior of the point of steepest concentration gradient qualitatively matches that of the inner boundary of the formalin band observed on the T_1 images (Fig. 2). The first two spatial derivatives of Eq. [13] are given by

$$\frac{\partial c}{\partial r} = \frac{2}{\pi}\sum_{n=1}^{\infty} -\frac{(-1)^n\sin[n\pi r]\exp[-n^2\pi^2 t]}{nr^2} + \frac{(-1)^n\cos[n\pi r]\pi\exp[-n^2\pi^2 t]}{r} \quad [14]$$

and

$$\frac{\partial^2 c}{\partial r^2} = \frac{2}{\pi}\sum_{n=1}^{\infty}\frac{2(-1)^n\sin[n\pi r]\exp[-n^2\pi^2 t]}{nr^3} - \frac{2(-1)^n\cos[n\pi r]\pi\exp[-n^2\pi^2 t]}{r^2} - \frac{(-1)^n\sin[n\pi r]n\pi^2\exp[-n^2\pi^2 t]}{r}, \quad [15]$$

so that the point at which Eq. [15] equals zero marks the inner boundary of the formalin band in this model. The measured normalized inner boundary of the formalin band and the zero of Eq. [15] both approach a nonzero asymptote in time. The theoretical asymptote is at $r = 0.6625$. So if the hypothesis that the inner boundary of the formalin band is marked by the location of the steepest concentration gradient is correct, we should observe a band that propagates inward to a fixed radius near $r = 0.66$ and then slowly fades away. Because the brain is not spherical and because the process of fixation involves more than simple diffusive mass transfer, the value of the band radius asymptote will be a little different from 0.6625. The diffusion model is, at best, a first-order model, so it was expected that the actual asymptote radius would be different from the model. So a correction, or second registration, of the brain in spherical coordinates to stretched spherical coordinates (in the radial direction) in which the radius of the asymptotes in the theoretical model and the transformed brain area data coincide was required. To compare the measured data to the model of the formalin band boundary, we converted the measured value of the normalized radius for each measured time point using a linear transformation so that the transformed normalized radii had an asymptotic value at 0.6625. Finally, the math model time at the transformed r (the zero solution to Eq. [15] at the given r) was computed and plotted with the measured time to reproduce the relation $t_1 = t/D$ where t_1 represents the model time and t represents the measured time. A linear regression through the plotted points then gave a value for D, the diffusion coefficient of formalin into the brain. This final linear regression brings the model back to that of Eq. [12].

RESULTS

A qualitative difference, as opposed to the quantitative differences in T_1, T_2, and PD, was only observed on the T_1-weighted images where the apparently formalin-fixed brain appeared as a lighter band that became progressively thicker with time as the formalin fixed deeper tissues. No setting of window level and width showed the band in any other images. Figure 3 demonstrates the enlarging formalin band at four time points.

Figure 4 illustrates how the signal was reduced, as the formalin progressively fixed the brain from outside inward, for all measured parameters except ADC, which remained more or less constant. The computed values of the exponential curve fits of Eq. [5] for T_1 relaxation, T_2 relaxation, and PD for gray and white matter in each ROI are shown in Table 1. Based on the fits given by Eq. [5] in ROI 4, using five time constants as the time to change, we observed the following changes from before fixation to

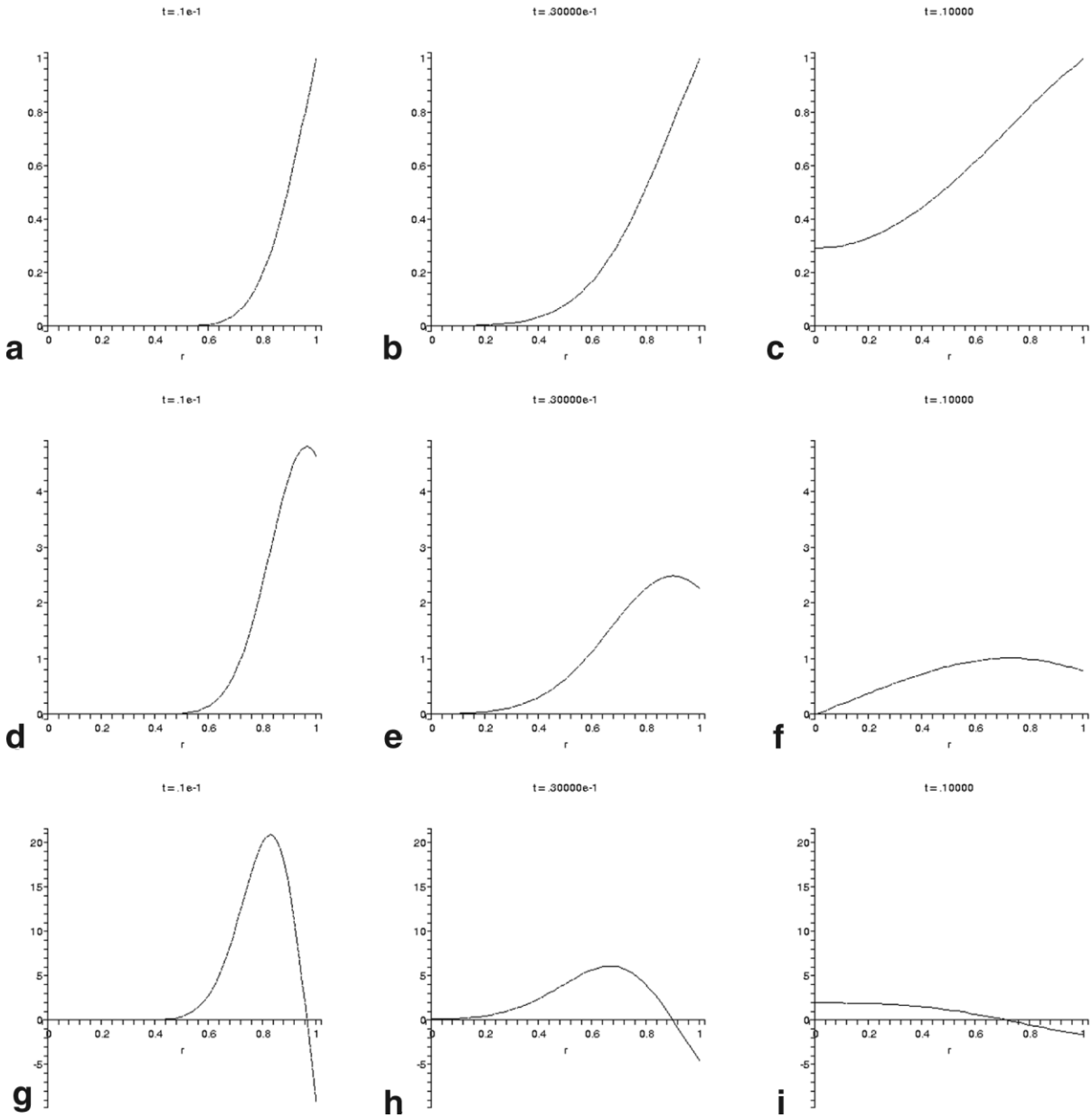

FIG. 2. Plots, as functions of radius and times $t = 0.01, 0.03, 0.10$, of the mathematical model of (**a–c**) normalized formalin concentration (corresponding to Eq. [13]), (**d–f**) the gradient of the formalin concentration (corresponding to Eq. [14]), and (**g–i**) the second radial derivative of the formalin concentration (corresponding to Eq. [15]). The location of the maximum of the concentration gradient may be easily seen as the points where the second radial derivative of the formalin concentration crosses the *r*-axis. These plots are frames from the computer animation mentioned in the text.

after complete fixation: T_1 decreased from 840 to 500 ms in white matter (40% change in 820 h) and from 1220 to 740 ms (39% change in 760 h) in gray matter; T_2 decreased from 80 to 40 ms in white matter (50% change in 770 h) and from 80 to 50 ms in gray matter (38% change in 1110 h); proton density decreased from 1440 to 1000 grayscale units in white matter (31% change in 750 h) and from 1810 to 1380 grayscale units in gray matter (24% change in 630 h); the ADC of gray and white matter remained constant at roughly 30×10^{-7} and 50×10^{-7} cm^2/s, respectively.

The exponential growth of the formalin band to an asymptote, calculated from a least squares curve fit to the ratio of formalin band area to the area of the rest of the brain, was determined to be

$$m = -0.66 \exp[-0.02\ t] + 0.66 \quad [16]$$

(correlation, $r = 0.988$, $P < 0.0001$) (Fig. 5a), while a similar fit to the same data presented as normalized radius (Fig. 5b) was

$$m = -0.58 \exp[-0.02\ t] + 0.58. \quad [17]$$

The comparison of theoretical times for the zeros of the second derivative of the formalin concentration spatial distribution with the measured times at corresponding formalin band inner normalized radii (Fig. 5c) gave a linear regression fit with a slope of 5.26×10^{-4} normalized radii per hour ($r = 0.93$). For a brain radius of 100 mm this

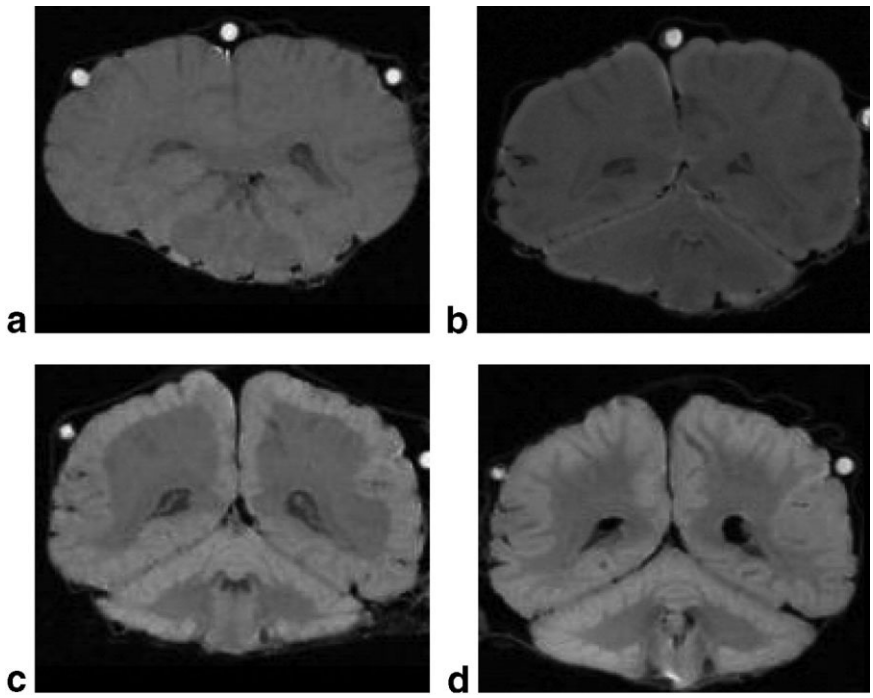

FIG. 3. T_1-weighted images of brain 2: (**a**) before formalin fixation and at (**b**) 18 h, (**c**) 90 h, and (**d**) 518 h. The apparently formalin-fixed tissue is visible as a light band that becomes progressively thicker with time. Mathematical modeling shows that the boundary of the band is likely to be where the formalin concentration gradient is steepest.

slope corresponds to a formalin diffusion rate, D, of approximately 52.6 mm^2/h.

DISCUSSION

Postmortem MR imaging is widely used in research. Formalin-fixed human brains have been scanned for pathologic diagnosis, neuroanatomical description and localization, embryologic and developmental studies and, recently, to examine cerebral vasculature. The results of our study show that the relaxation coefficients and proton density value, as well as the appearance of the entire brain, change with progressive formalin fixation. The apparent water self-diffusion coefficient remains more or less constant at approximately 40 $\times$ 10^{-7} cm^2/s with formalin fixation. A study of mouse brains (9) found the ADC to drop from approximately 200 $\times$ 10^{-7} cm^2/s in live animals to approximately 80 $\times$ 10^{-7} cm^2/s in formalin-fixed

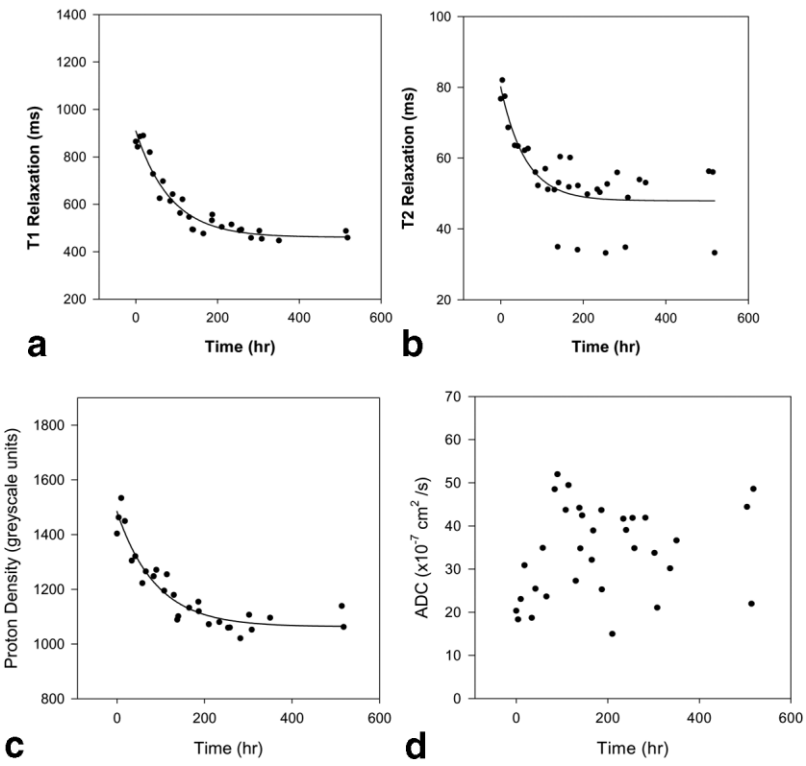

FIG. 4. Typical ROI time series courses and exponential curve fits for white matter imaging parameters. (**a**) T_1. (**b**) T_2. (**c**) PD. (**d**) ADC (see Table 1 for details). The ADC value remained more or less constant. The time courses in all ROIs for both gray and white matter were qualitatively similar to the ones shown here.

Table 1
Parameters From the Fit of $y = a_1 (1 - \exp(-a_2 t)) + a_3$ to individual ROIs

ROI[a]	a_3[†]				$a_1 + a_3$[†]				$5/a_2$[†]			
	1	2	3	4	1	2	3	4	1	2	3	4
T_1 white matter[b]	1222	908	849	844	799	450	458	497	121	424	862	820
T_1 gray matter[b]	1174	1351	1290	1220	784	635	394	740	262	526	1724	758
T_2 white matter[b]	77	80	84	83	63	48	45	44	29	877	500	769
T_2 gray matter[b]	[e]	84	84	82		59	51	51		485	877	1111
PD white matter[c]	1805	1484	1444	1441	1462	1063	1045	1002	116	442	595	746
PD gray matter[c]	1725	1853	1821	1808	1456	1427	1249	1379	1111	568	1471	625

[a]ROI 1 is the most superficial while ROI 4 is the deepest.
[b]Units for a_1 and a_3 = msec for $5/a_2$ = h.
[c]Units for a_1 and a_3 = grayscale; for $5/a_2$ = h.
[d]For all parameters, $P < 0.01$.
[e]The empty table cells are where the values were essentially constant.
[†]a_3 represents the value at time zero, $a_1 + a_3$ represents the asymptotic value, and $1/a_2$ is the time constant so that the values are 99% converged to $a_1 + a_3$ after $5/a_2$.

brains. One possible explanation of this apparent discrepancy with our conclusion, aside from the large noise component in our data due to the low b value, is that the ADC change observed in the mouse brain was due to death and not to formalin fixation. The difference between live and fresh dead brains may be another reason, apart from a random bias due to uncontrolled gain during image acquisition, why the T_1 values for gray and white matter at the beginning of our curves (e.g., Fig. 4) are higher than other published T_1 values (10).

We observed the formation of a lighter formalin band in T_1-weighted images on the outer boundary of the brain that increased in thickness with time of formalin fixation. It is not known why the band does not appear in other images (e.g., in T_2-weighted images) and other contrasts (e.g., inversion recovery) may also show the band. However, the progression of the inner boundary of the band was consistent with the progression of the steepest part of the formalin concentration gradient into the brain as the formalin diffused into the brain. This process that we have modeled as simple diffusion was, in actuality, likely a combination of diffusion followed by tissue fixation. However, the simple analytic diffusion model closely modeled the progression of the lighter band of tissue seen in the T_1-weighted images into the brain. Deviations from the fitted line in Fig. 5 are likely due to the fact that the human brain is not a solid sphere and also to the fact that formalin fixation is a chemical process in addition to a strictly diffusive one. The diffusion model is, nevertheless, clearly a good first-order approximation of the progression of formalin fixation, especially in modeling the feature that the location of the steepest concentration gradient asymptotically approaches a nonzero radius in time.

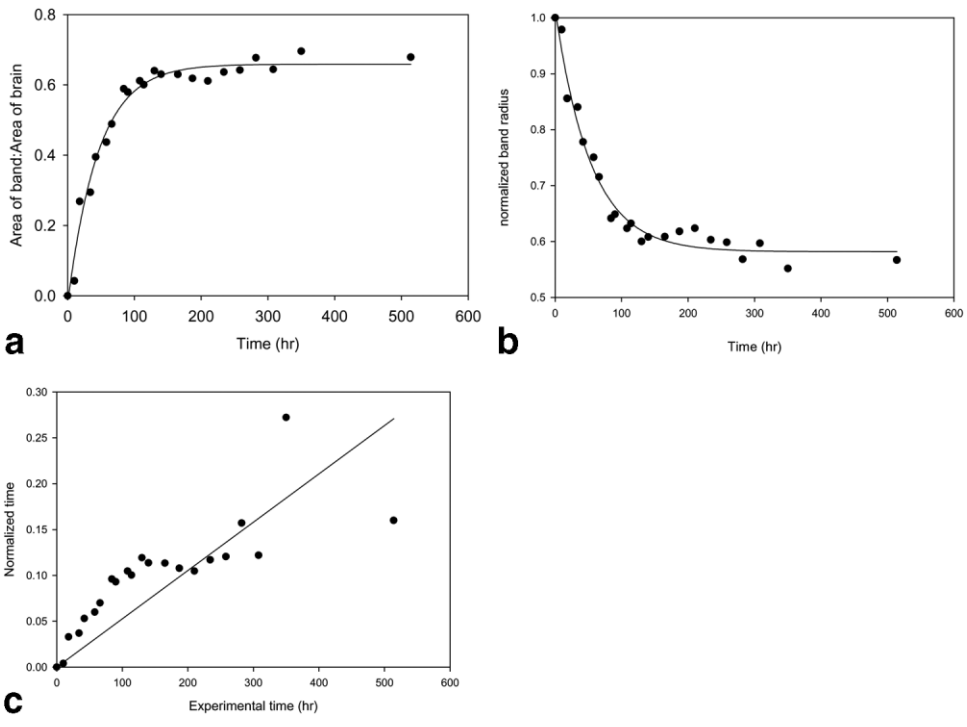

FIG. 5. The ratio of formalin-fixed brain area to the rest of the brain area increases exponentially to a nonunit limit. (**a**) The measured ratios of the formalin band area to the whole brain area for the selected image slice, averaged over three brains. (**b**) The measured ratios converted to a normalized radius r with $0 \leq r \leq 1$. (**c**) Comparison of measured normalized formalin band radius with theoretical values for a unit diffusion rate. The slope of the fitted line is approximately 52.6 mm^2/h (see text).

Investigators using formalin-fixed brain tissue must be cautious when making inferences based on relaxation rate or image contrast, including the identification of gray and white matter. Many studies compare and correlate histopathology to MR imaging findings. For example, a number of groups have examined signal changes in the pathologic substrate of postmortem brains of patients with multiple sclerosis (MS) using MR imaging. While some of these studies have used unfixed brain (11–14), others have used fixed brain (15–18). A more recent comprehensive study used both fresh and fixed specimens to develop a technique for the coregistration of signal changes visible on MR imaging and their correlates in postmortem brains from patients with MS (19). Postmortem MR imaging has also been used to evaluate formalin-fixed brains of patients with Alzheimer's disease (20–23), amyotrophic lateral sclerosis (23), and AIDS (24,25). One case report describes the postmortem MR imaging findings, using a formalin-fixed brain, in a pediatric patient with no prior known brain pathology (26). Thus, numerous postmortem studies are attempting to use various MRI parameters to describe disease progression.

Specific areas of the brain have also been examined using postmortem MR imaging of normal patients using formalin fixation. The primary auditory cortex (27) and the primary somatosensory cortex (28) have been mapped; the appearance of the mammilothalamic tract (29), the microstructural architecture of the corpus callosum (30), and the internal architecture of Ammon's horn (31) have been described; identification of hippocampal layers has been achieved (32). In addition, MR imaging volumetry has been reported using both normal and pathologic postmortem formalin-fixed brains (27,33–35).

Recently, postmortem MR imaging of formalin-fixed brains has been used to study cerebral vasculature. That recent study described microbleeds in postmortem MR imaging of patients who had no prior in vivo studies for correlation (36). Areas of signal loss on gradient echo T_2-weighted images were shown to indicate previous extravasation of blood related to bleeding-prone microangiopathy of different origins in another study (37). However, small vessels seen in vivo and in the unfixed brain could not be visualized after fixation in a recent study comparing the microvasculature of live and fixed brains (38).

MR imaging of postmortem fetal and still-born neonate brains have provided information of the embryological development of the central nervous system (39). A volumetric study of fixed postmortem fetuses quantified postmortem shrinkage and described the volumetric development of the germinal matrix and ventricles (40).

Our study demonstrated changes in MR signal that progressed with time of fixation. Investigators currently do not consistently report the time after fixation that the images were acquired, making comparison and accurate interpretation of the results difficult. A number of factors can influence fixation, including the type of fixation, volume of material to be fixed, presence or absence of pathology, and the age of the tissue. Findings could also be affected by the degree of fixation in studies where the value of relaxation parameters are used for diagnosis and where anatomic localization is based on contrast. Postmortem MR volumetry is unlikely to be confounded by MR signal change from fixation; however, it is important to note that various fixation methods are known to "shrink " brain tissue. Other as yet unrecognized changes in brain tissue also likely occur. Further research is needed and researchers should be aware of the potential for misinterpretation of formalin-fixed MR images of the brain.

The reduction in T_2 relaxation demonstrated here is in keeping with previously reported results (5). In addition to reduction in T_2 signal, we found significant reduction in T_1 relaxation and PD signals with progressive formalin fixation and quantified the change in the light band of formalin-fixed tissue, previously described as artifact (5).

The time constant of the exponential decay of the formalin band to a fixed radius is 50 h (1/0.02). As a rule of thumb, an exponential decay may be considered to have reached its asymptote in five time constants, or 250 h in this case. The inner boundary of the light formalin band approached its asymptotic normalized radius of 0.58 and then the contrast between the band and the rest of the brain faded in accordance with a mathematical model of the formalin concentration gradients. The last time point measured, 514 h of fixation (see Fig. 2d), corresponds to a normalized model time of approximately 0.2. Therefore, the model predicts that formalin diffusion is not complete, and the light formalin band not completely faded, until after 2500 h (14.8 weeks) of fixation. Given the simple model of formalin diffusion used here, 2500 h may be an overestimate. For example, the formalin diffusion coefficient may change between gray and white matter. If the diffusion coefficient for white matter is higher, then the fixation will proceed faster after the outer gray matter has been fixed. One way to model such a diffusion coefficient change would be to model the brain as two concentric spheres with the inner sphere representing white matter and the outer sphere (minus the inner sphere) representing gray matter. The time resolution of our data points in Fig. 5c for the later time points prevents us from applying the two-sphere model to our data but future experiments, perhaps with smaller animal brains to reduce the fixation time, might be compared to a two-sphere model. Also, the time to fixation may be different than the time to complete formalin diffusion into the brain. Fixation likely occurs when the tissue has been exposed to a high enough concentration of formalin for a long enough period of time. The data of Table 1 suggest that, for the initial concentration of 20% phosphate buffered formalin, roughly 900 h (5.4 weeks) is required for complete fixation. Nevertheless, while the true fixation time may be less than 2500 h, the fixation time is long so investigators should consistently report the duration of fixation at the time MR images are acquired and to consider the effects of incomplete fixation in order to avoid artificial results, misinterpretation, and misdiagnosis.

CONCLUSION

T_1 and T_2 relaxation rates and proton density all decreased in both gray and white matter with formalin fixation. ADC was found to remain relatively constant as formalin fixation of the brain progressed. In addition, a lighter formalin band was observed near the surface of brain in T_1-weighted images that widens as fixation progressed. The inner boundary of the formalin band, previously unexplained, was at a location consistent with a mathematical

model of the steepest part of the formalin concentration gradient. All of these changes lead to contrast change in postmortem MR images of formalin-fixed brains. Investigators in forensic and clinical pathology, who image formalin-fixed brains, must be aware of these MR signal changes when interpreting the images.

ACKNOWLEDGMENTS

The technical assistance of Jennifer Hadley for data analysis and the assistance of David George in obtaining the cadaver brains are gratefully acknowledged.

REFERENCES

1. Kamman RL, Go KG, Stomp GP, Hulstaert CE, Berendsen HJ. Changes of relaxation times T_1 and T_2 in rat tissues after biopsy and fixation. Magn Reson Imaging 1985;3:245–250.
2. Thickman DI, Kundel HL, Wolf G. Nuclear magnetic resonance characteristics of fresh and fixed tissue: the effect of elapsed time. Radiology 1983;148:183–185.
3. Carvlin MJ, Asato R, Hackney DB, Kassab E, Joseph PM. High-resolution MR of the spinal cord in humans and rats. Am J Neuroradiol 1989;10:13–17.
4. Pattany PM, Puckett WR, Klose KJ, Quencer RM, Bunge RP, Kasuboski L, Weaver RG. High-resolution diffusion-weighted MR of fresh and fixed cat spinal cords: evaluation of diffusion coefficients and anisotropy. Am J Neuroradiol 1997;18:1049–1056.
5. Blamire AM, Rowe JG, Styles P, McDonald B. Optimising imaging parameters for post mortem MR imaging of the human brain. Acta Radiol 1999;40:593–597.
6. Hallam DK. Miscellaneous brain pathology. In Haacke EM, Lin W, et al., editors. Current protocols in magnetic resonance imaging. New York: Wiley, 2002. Section A5.
7. Fick A. Uber diffusion. Ann Phys Chem 1855;94:59–86.
8. Zachmanoglou EC, Thoe DW. Introduction to partial differential equations with applications. New York: Dover, 1986. p 352.
9. Sun S-W, Neil JJ, Song S-K. Relative indices of water diffusion anisotropy are equivalent in live and formalin-fixed mouse brains. Magn Reson Med 2003;743–748.
10. Gowland PA, Stevenson VL. T1: the longitudinal relaxation time. In Tofts P, editor. Quantitative MRI of the brain: measuring changes caused by disease. Hoboken, NJ: Wiley; 2003. p 111–141.
11. De Groot CJ, Bergers E, Kamphorst W, Ravid R, Polman CH, Barkhof F, van der Valk P. Post-mortem MR imaging-guided sampling of multiple sclerosis brain lesions: increased yield of active demyelinating and (p)reactive lesions. Brain 2001;124:1635–1645.
12. Newcombe J, Hawkins CP, Henderson CL, Patel HA, Woodroofe MN, Hayes GM, Cuzner ML, MacManus D, du Boulay EP, McDonald WI. Histopathology of multiple sclerosis lesions detected by magnetic resonance imaging in unfixed postmortem central nervous system tissue. Brain 1991;114:1013–1023.
13. van Waesberghe JH, Kamphorst W, De Groot CJ, van Walderveen MA, Castelijns JA, Ravid R, Lycklama a Nijeholt GJ, van der Valk P, Polman CH, Thompson AJ, Barkhof F. Axonal loss in multiple sclerosis lesions: magnetic resonance imaging insights into substrates of disability. Ann Neurol 1999;46:747–754.
14. van Walderveen MA, Kamphorst W, Scheltens P, van Waesberghe JH, Ravid R, Valk J, Polman CH, Barkhof F. Histopathologic correlate of hypointense lesions on T_1-weighted spin-echo MRI in multiple sclerosis. Neurology 1998;50:1282–1288.
15. Moore GR, Leung E, MacKay AL, Vavasour IM, Whittall KP, Cover KS, Li DK, Hashimoto SA, Oger J, Sprinkle TJ, Paty DW. A pathology-MRI study of the short-T_2 component in formalin-fixed multiple sclerosis brain. Neurology 2000;55:1506–1510.
16. Kidd D, Barkhof F, McConnell R, Algra PR, Allen IV, Revesz T. Cortical lesions in multiple sclerosis. Brain 1999;122:17–26.
17. Barkhof F, Scheltens P, Kamphorst W. Pre-and post-mortem MR imaging of unsuspected multiple sclerosis in a patient with Alzheimer's disease. J Neurol Sci 1993;117:175–178.
18. Macchi G, Cioffi RP. An in vivo and post mortem MRI study in multiple sclerosis with pathological correlation. Ital J Neurol Sci 1992;13:97–103.
19. Schmierer K, Scaravilli F, Barker GJ, Gordon R, MacManus DG, Miller DH. Stereotactic co-registration of magnetic resonance imaging and histopathology in post-mortem multiple sclerosis brain. Neuropathol Appl Neurobiol 2003;29:596–601.
20. Bronge L, Bogdanovic N, Wahlund LO. Postmortem MRI and histopathology of white matter changes in Alzheimer brains. A quantitative, comparative study. Dement Geriatr Cogn Disord 2002;13:205–212.
21. Dhenain M, Privat N, Duyckaerts C, Jacobs RE. Senile plaques do not induce susceptibility effects in T_2*-weighted MR microscopic images. NMR Biomed 2002;15:197–203.
22. Bobinski M, de Leon MJ, Wegiel J, Desanti S, Convit A, Saint Louis LA, Rusinek H, Wisniewski HM. The histological validation of post mortem magnetic resonance imaging-determined hippocampal volume in Alzheimer's disease. Neuroscience 2000;95:721–725.
23. Abe K, Fujimura H, Kobayashi Y, Fujita N, Yanagihara T. Degeneration of the pyramidal tracts in patients with amyotrophic lateral sclerosis. A premortem and postmortem magnetic resonance imaging study. J Neuroimaging 1997;7:208–212.
24. Scatliff JH, Kwock L, Chancellor K, Bouldin TW, Kapoor CC, Castillo M. Postmortem MR imaging of the brains of patients with AIDS. Neuroimaging Clin N Am 1997;7:297–320.
25. Everall IP, Chong WK, Wilkinson ID, Paley MN, Chinn RJ, Hall-Craggs MA, Scaravilli F, Lantos PL, Luthert PJ, Harrison MJ. Correlation of MRI and neuropathology in AIDS. J Neurol Neurosurg Psychiatry 1997; 62:92–95.
26. Quan L, Zhu BL, Ishida K, Taniguchi M, Li DR, Kamikodai Y, Fujita MQ, Maeda H. Sudden death of an infant with early epileptic encephalopathy. Forens Sci Int 2001;124:62–67.
27. Rademacher J, Morosan P, Schormann T, Schleicher A, Werner C, Freund HJ, Zilles K. Probabilistic mapping and volume measurement of human primary auditory cortex. Neuroimage 2001;13:669–683.
28. Geyer S, Schormann T, Mohlberg H, Zilles K. Areas 3a, 3b, and 1 of human primary somatosensory cortex. Part 2. Spatial normalization to standard anatomical space Neuroimage 2000;11:684–696.
29. Yamada K, Shrier DA, Rubio A, Yoshiura T, Iwanaga S, Shibata DK, Patel U, Numaguchi Y. MR imaging of the mamillothalamic tract. Radiology 1998;207:593–598.
30. Chepuri NB, Yen YF, Burdette JH, Li H, Moody DM, Maldjian JA. Diffusion anisotropy in the corpus callosum. Am J Neuroradiol 2002; 23:803–808.
31. Miller MJ, Mark LP, Ho KC, Haughton VM. MR appearance of the internal architecture of Ammon's horn. Am J Neuroradiol 1996;17:23–26.
32. Wieshmann UC, Symms MR, Mottershead JP, MacManus DG, Barker GJ, Tofts PS, Revesz T, Stevens JM, Shorvon SD. Hippocampal layers on high resolution magnetic resonance images: real or imaginary?. J Anat 1999;195:131–135.
33. Selemon LD, Kleinman JE, Herman MM, Goldman-Rakic PS. Smaller frontal gray matter volume in postmortem schizophrenic brains. Am J Psychiatry 2002;159:1983–1991.
34. Chance SA, Esiri MM, Crow TJ. Ventricular enlargement in schizophrenia: a primary change in the temporal lobe?. Schizophr Res 2003;62:123–131.
35. Cotter D, Miszkiel K, Al-Sarraj S, Wilkinson ID, Paley M, Harrison MJ, Hall-Craggs MA, Everall IP. The assessment of postmortem brain volume; a comparison of stereological and planimetric methodologies. Neuroradiology 1999;41:493–496.
36. Messori A, Salvolini U. Postmortem MRI as a useful tool for investigation of cerebral microbleeds. Stroke 2003;34:376–377.
37. Fazekas F, Kleinert R, Roob G, Kleinert G, Kapeller P, Schmidt R, Hartung HP. Histopathologic analysis of foci of signal loss on gradient-echo T_2*-weighted MR images in patients with spontaneous intracerebral hemorrhage: evidence of microangiopathy-related microbleeds. Am J Neuroradiol 1999;20:637–642.
38. Dashner RA, Chakeres DW, Kangarlu A, Schmalbrock P, Christoforidis GA, DePhilip RM. MR imaging visualization of the cerebral microvasculature: a comparison of live and postmortem studies at 8 T. Am J Neuroradiol 2003;24:1881–1884.
39. Griffiths PD, Variend D, Evans M, Jones A, Wilkinson ID, Paley MNJ, Whitby E. Postmortem MR imaging of the fetal and stillborn central nervous system. Am J Neuroradiol 2003;24:22–27.
40. Kinoshita Y, Okudera T, Tsuru E, Yokota A. Volumetric analysis of the germinal matrix and lateral ventricles performed using MR images of postmortem fetuses. Am J Neuroradiol 2001;22:382–388.